**Supplementary Information**

# AKAP5 complex facilitates purinergic modulation of vascular L-type $Ca^{2+}$ channel $Ca_V1.2$

Maria Paz Prada[1]*, Arsalan U. Syed[1]*, Gopireddy R. Reddy[1]*, Miguel Martín-Aragón Baudel[1], Víctor A. Flores-Tamez[1], Kent C. Sasse[2], Sean M. Ward[3], Padmini Sirish[4], Nipavan Chiamvimonvat[1, 4, 5], Peter Bartels[1], Eamonn J. Dickson[6], Johannes W. Hell[1], John D. Scott[7], Luis F. Santana[6], Yang K. Xiang[1, 5], Manuel F. Navedo[1], and Madeline Nieves-Cintrón[1]

[1]Department of Pharmacology, University of California Davis, Davis, CA, USA 95616, [2]Sasse Surgical Associates, Reno, NV, USA 89502, [3]Department of Physiology and Cell Biology, University of Nevada Reno, Reno, NV, USA 89557, [4]Department of Internal Medicine, University of California Davis, Davis, CA, USA 95616, [5]VA Northern California Healthcare System, Mather, CA, USA 95655, [6]Department of Physiology and Membrane Biology, University of California Davis, Davis, CA, USA 95616, and [7]Department of Pharmacology, University of Washington Seattle, Seattle, WA, USA 98195

**Supplemental Figures and Tables**

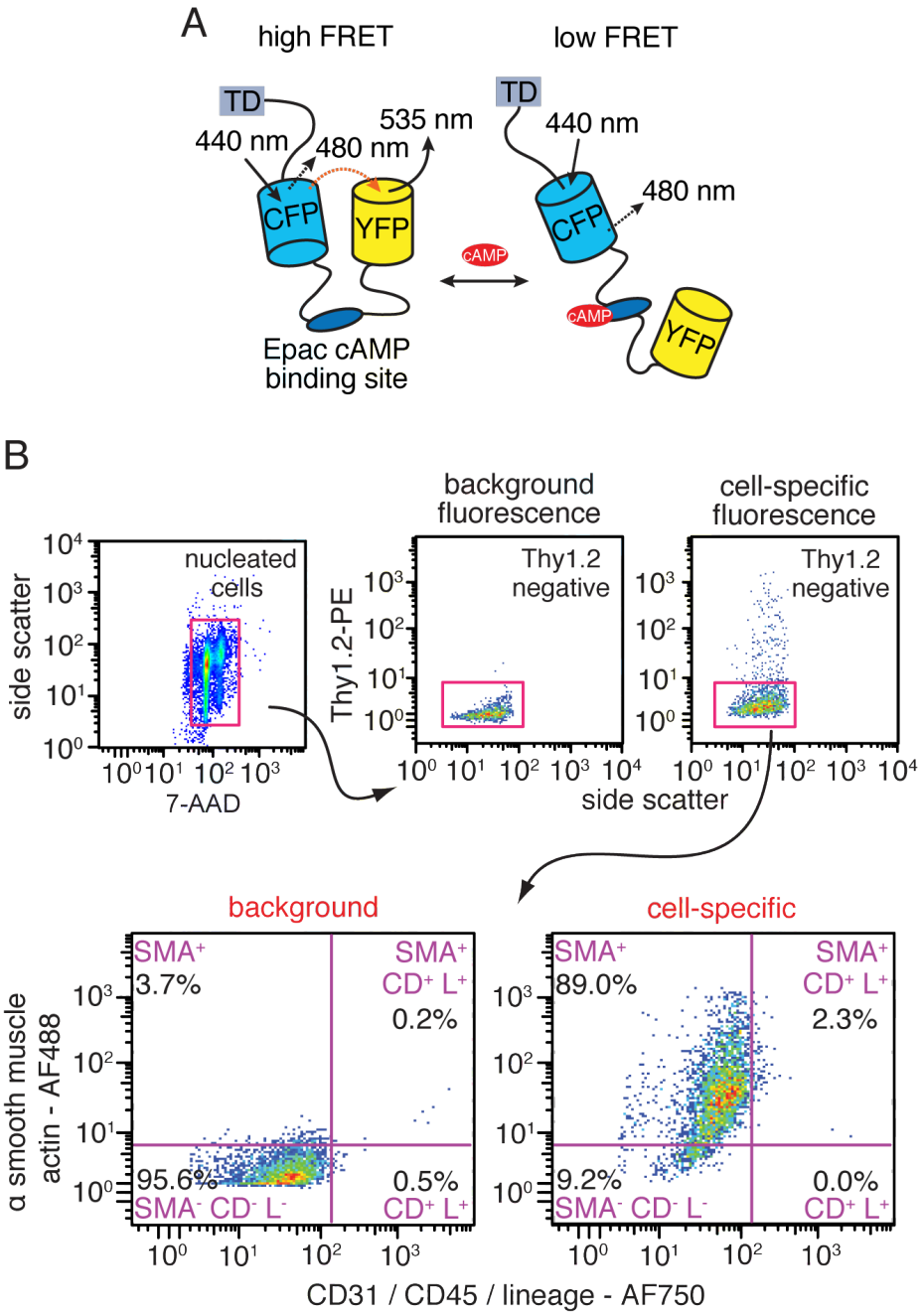


**Supplementary Figure 1: Diagram of the ICUE3-PM sensor and flow cytometry analysis of unpassaged primary cultured arterial myocytes. A)** Schematic of the design for the plasma membrane-targeted Epac1-camps-based FRET sensor (ICUE3-PM). TD = targeting domain. **B)** Flow cytometry analysis of arterial myocytes (α-

$SMA^{+}$/$Thy^{-}$/$CD31^{-}$/$CD45^{-}$/$Lin^{-}$). Nucleated cells were selected from the mixed population based on the incorporation of 7-AAD (top left panel). Selection of non-fibroblasts ($Thy1.2^{neg}$) are shown in the top middle and right panels. Arterial myocytes were identified as $CD31^{-}$/$CD45^{-}$/lineage negative and α-smooth muscle actin positive in the bottom panels. X and Y-axes represent arbitrary units. Representative results are shown (n = 4 preparations). Source data are provided as Source Data file.

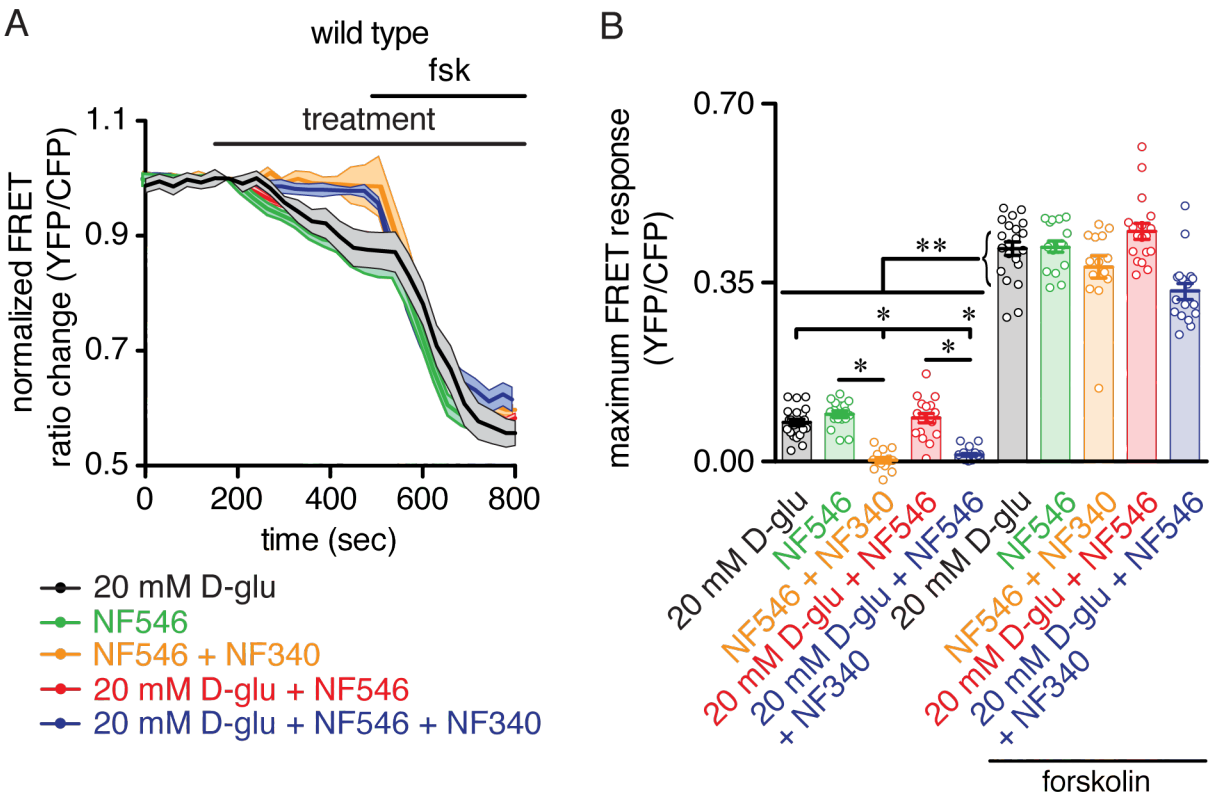


**Supplementary Figure 2: NF340 prevents glucose/NF546-induced cAMP synthesis. A)** Time courses of averaged ICUE3-PM traces (mean = solid line; SEM = shadow) in wild type (WT) arterial myocytes in response to 20 mM D-glucose (D-glu; black; n = 21 cells/6 mice), 500 nM NF546 (green; n = 17 cells/6 mice), and 20 mM D-glu + NF546 (red; n = 18 cells/6 mice) and after application of 1 µM forskolin. In a set of experiments, cells were first pretreated with the $P2Y_{11}$ antagonist NF340 (10 µM) before applying 500 nM NF546 (orange; n = 14 cells/6 mice) and 20 mM D-glucose + NF546 (blue; n = 17 cells/6 mice). Horizontal bar indicates treatment. **B)** Plot of maximum FRET responses (YFP/CFP) for arterial myocytes in response to the indicated treatment. *$P$ < 0.05 with Kruskal-Wallis One-way ANOVA with Dunn's multiple comparisons. The single asterisks highlight significant differences between datasets in the absence of forskolin. The double asterisks indicate a statistical difference within the same experimental group in the absence and presence forskolin. $P$ = 0.0003 for 20 mM D-glu-20 mM D-glu + NF546 + NF340, and all other significant $P$ values are < 0.0001. Data represent mean ± SEM. Source data are provided as Source Data file.

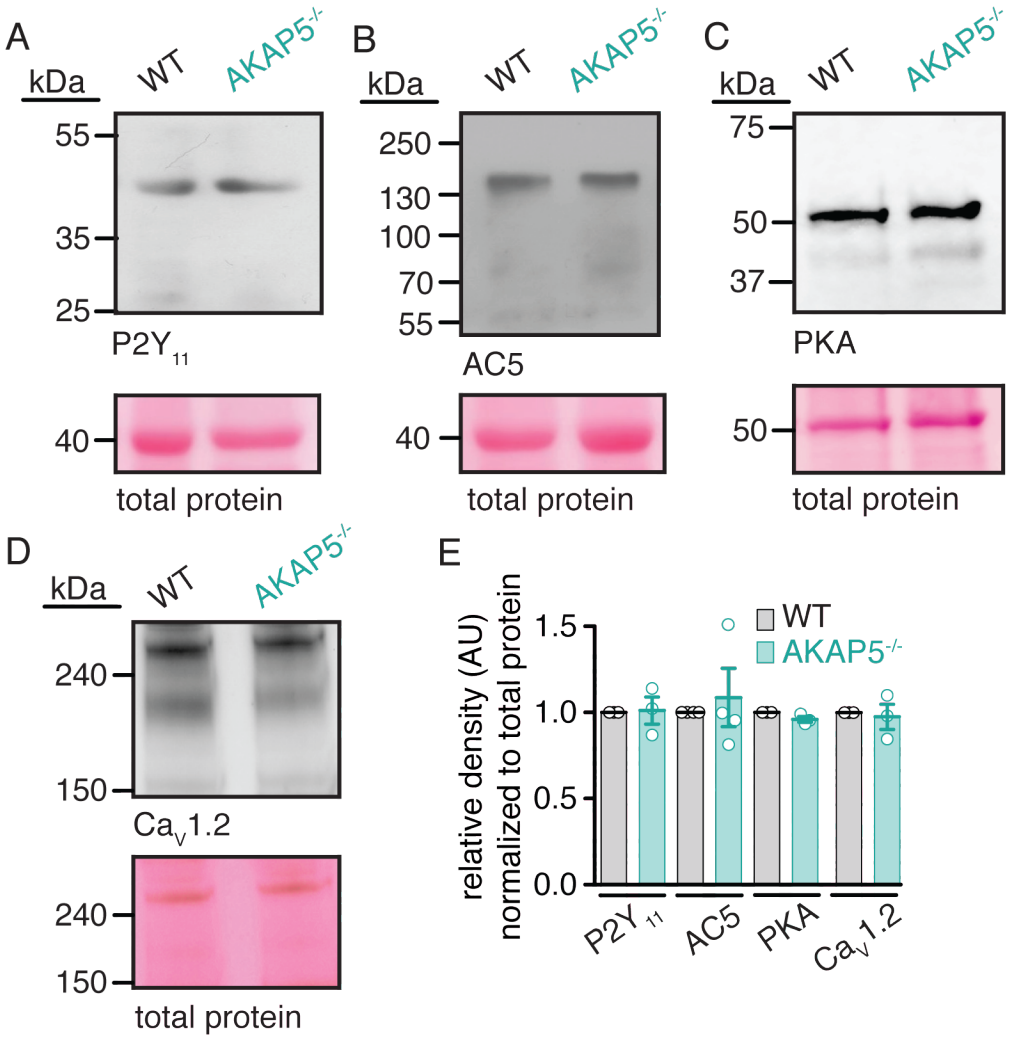


**Supplementary Figure 3: Similar $P2Y_{11}$, AC5, PKA and $Ca_V1.2$ protein abundance in WT and AKAP5$^{-/-}$ lysates.** Representative Western blot of immunoreactive bands of expected molecular mass for **A**) $P2Y_{11}$ (~40 kDa), **B**) AC5 (~130 kDa), **C**) PKA (~50 kDa) and **D**) $Ca_V1.2$ (~240 kDa) in wild type (WT) and AKAP5$^{-/-}$ lysates. Ponceau staining was used for normalization of samples to total protein. **E**) Amalgamated densitometry data for $P2Y_{11}$ (n = 3 lysates/3 mice), AC5 (n = 4 lysates/4 mice), PKA (n = 3 lysates/3 mice) and $Ca_V1.2$ (n = 3 lysates/3 mice) in WT and AKAP5$^{-/-}$ lysates. *$P$ < 0.05 with two-tailed Mann-Whitney test comparing results between WT and AKAP5$^{-/-}$ samples. Data represent mean ± SEM. Source data are provided as Source Data file.

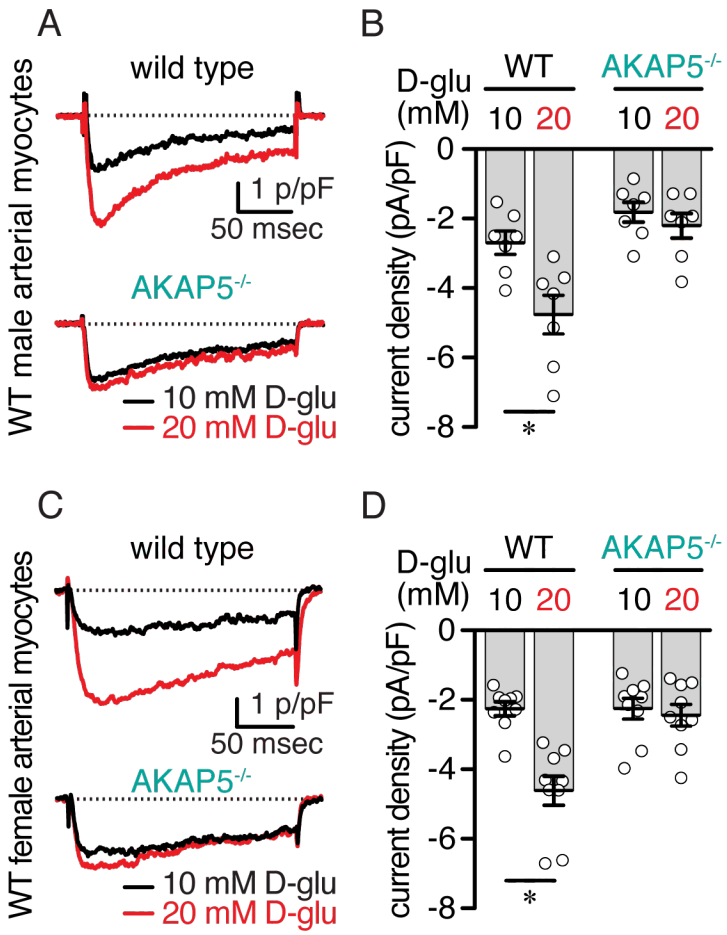


**Supplementary Figure 4. AKAP5 is required for glucose-induced L-type $Ca^{2+}$ channel potentiation in mouse male and female arterial myocytes.** Representative $Ba^{2+}$ currents ($I_{Ba}$) recordings and summary $I_{Ba}$ data of cerebral arterial myocytes from wild type (WT) and AKAP5$^{-/-}$ **A, B)** male (n = 7 cells/5 WT mice and n = 7 cells/4 AKAP5$^{-/-}$ mice) and **C, D)** female (n = 9 cells/3 WT mice and n = 9 cells/3 AKAP5$^{-/-}$ mice) mice evoked by step depolarizations from -70 to +10 mV in the presence of 10 mM or 20 mM D-glucose (D-glu). Dotted lines reflect baseline. *$P$ < 0.05 with two-tailed Wilcoxon test. Comparisons between the 10 mM and 20 mM D-glu condition for each dataset. $P$ = 0.0156 for WT male 10 mM D-glu-20 mM D-glu and $P$ = 0.0039 for WT female 10 mM D-glu-20 mM D-glu. Data represent mean ± SEM. Source data are provided as Source Data file.

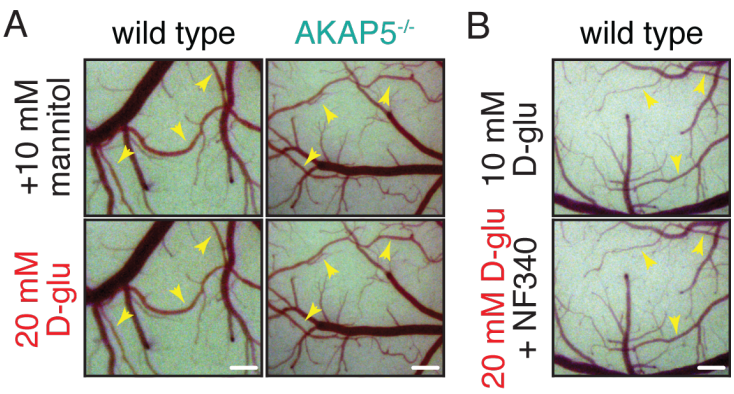


**Supplementary Figure 5. Exemplary images of cerebral arteries visualized through a cranial window in WT and AKAP5$^{-/-}$ mice.** Representative images of middle cerebral arteries and branches visualized through an open cranial window used to analyze diameter changes in response to **A)** 10 mM D-glucose (D-glu) + 10 mM mannitol and 20 mM D-glu in wild type (WT) and AKAP5$^{-/-}$ mice and **B)** 10 mM D-glu and 20 mM D-glu + NF340 in WT mice. Yellow arrows point to arteries. Scale bars = 50 pixels.

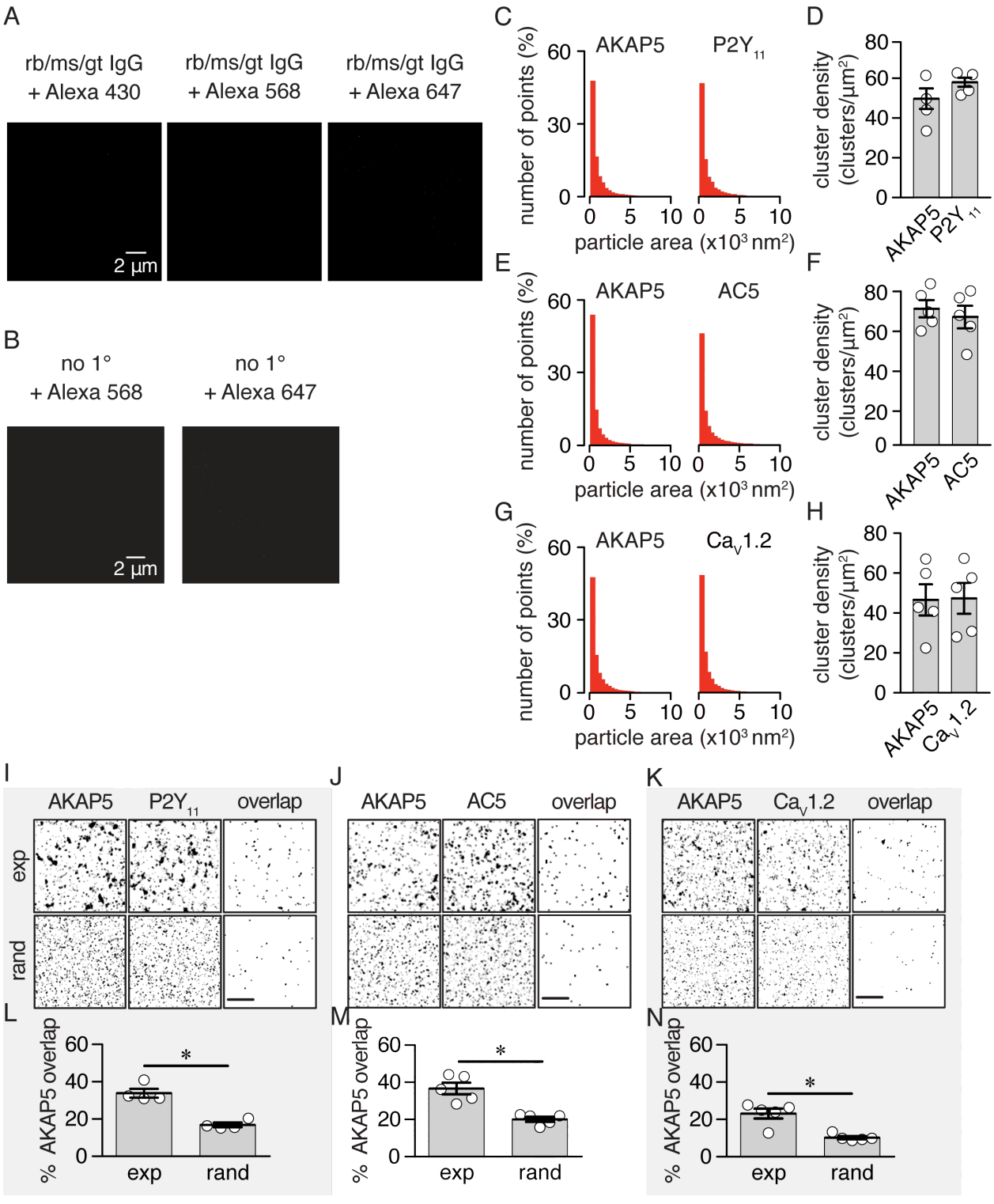


**Supplementary Figure 6: Negative controls for Airyscan and GSD super-resolution imaging, particle area and cluster density analysis, and protein overlap analysis. A)** Representative Airyscan images of an arterial myocyte triple labeled with

primary rabbit (rb), mouse (ms) and goat (gt) immunoglobulin G (IgGs) and secondary Alexa 430, Alexa 568 and Alexa 647 antibodies. Similar results were observed in 5 different cells from 2 mice. **B)** Exemplary Ground State Depletion (GSD) reconstruction maps of an arterial myocyte labeled only with secondary antibodies (no 1° + Alexa 568 and no 1° + Alexa 647). Similar results were observed in 7 different cells. Histograms of the cluster area and scatter plot of the cluster density of AKAP5 and $P2Y_{11}$ (**C, D**; n = 4 cells), AKAP5 and AC5 (**E, F**; n = 5 cells) and AKAP5 and $Ca_V1.2$ (**G, H**; n = 5 cells). Average cluster area for each dataset are **C)** AKAP5 = 2408 ± 46, $P2Y_{11}$ = 2697 ± 58, **E)** AKAP5 = 2721 ± 252, AC5 = 3514 ± 304 and **G)** AKAP5 = 2752 ± 52, $P2Y_{11}$ = 2093 ± 31. Representative experimental (exp; *top*) and randomized (rand; *bottom*) images of reconstruction maps for **I)** AKAP5-$P2Y_{11}$ (n = 4 cells), **J)** AKAP5-AC5 (n = 5 cells) and **K)** AKAP5-$Ca_V1.2$ (n = 5 cells). Scatter plots of percentage of overlap of AKAP5 with **L)** $P2Y_{11}$, **M)** AC5 and **N)** $Ca_V1.2$ for experimental and randomized simulation images. *$P$ < 0.05 with two-tailed Mann-Whitney test. $P$ = 0.0286 for AKAP5-$P2Y_{11}$, $P$ = 0.0079 for AKAP5-AC5 and $P$ = 0.0159 for AKAP5-$Ca_V1.2$. Data represent mean ± SEM. Source data are provided as Source Data file.

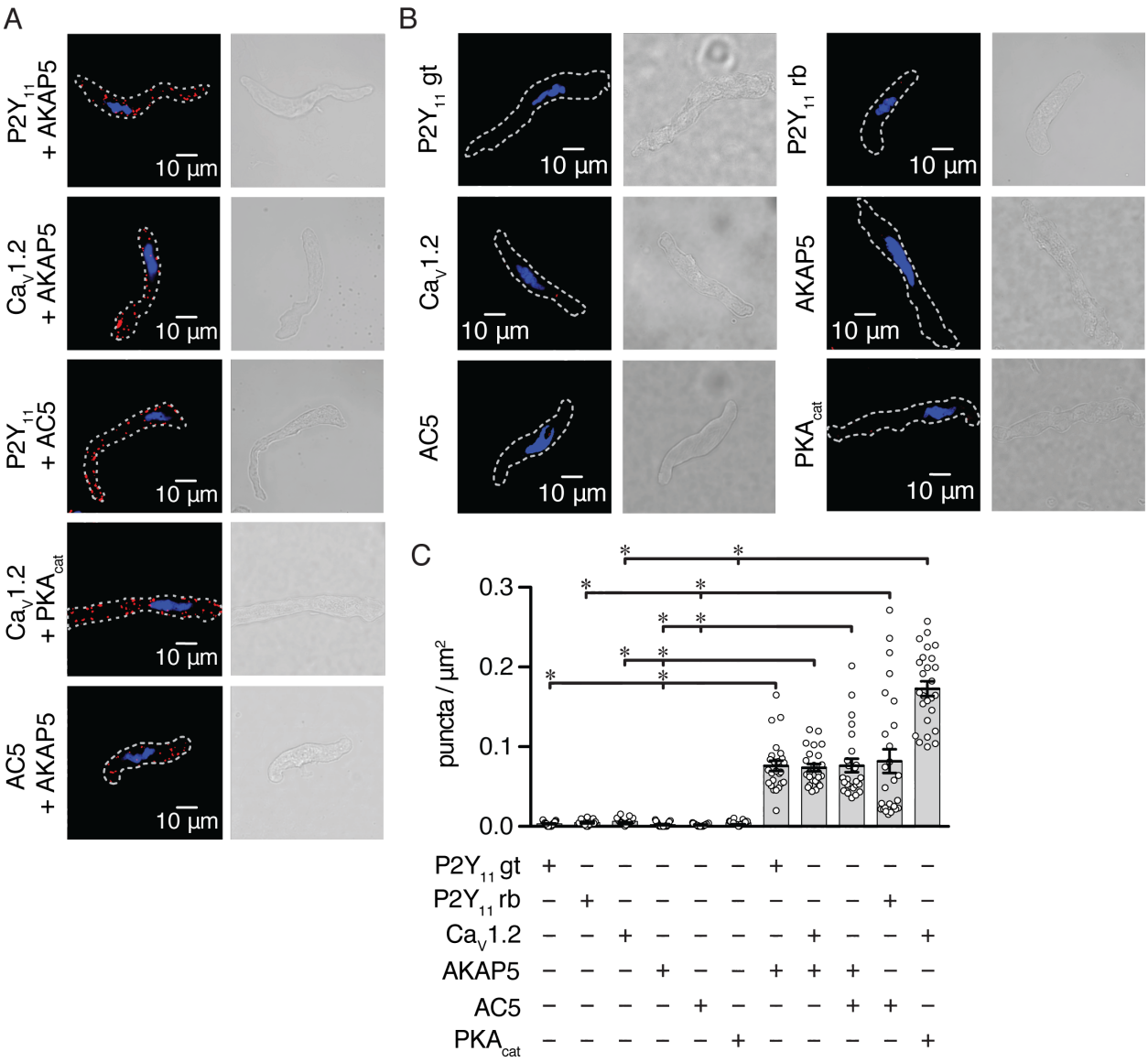


**Supplementary Figure 7. An AKAP5/$P2Y_{11}$/AC5/PKA/$Ca_V1.2$ nanocomplex in human arterial myocytes. A)** Representative merged fluorescence proximity ligation assay (PLA; red)/nucleus (blue; left panels) and differential interference contrast (right panels) images of human arterial myocytes co-labeled for **A)** $P2Y_{11}$ + AKAP5, $Ca_V1.2$ + AKAP5, $P2Y_{11}$ + AC5, $Ca_V1.2$ + $PKA_{cat}$ and AC5 + AKAP5, as well as representative images of cells labeled with only one 1° antibody for **B)** $P2Y_{11}$ (goat = gt), $P2Y_{11}$ (rabbit = rb), $Ca_V1.2$, AKAP5, AC5 and $PKA_{cat}$. **C)** Quantification of PLA fluorescent puncta per cell area (puncta/µm$^2$) for human arterial myocytes labeled for $P2Y_{11}$ gt (n = 27 cells/3 humans), $P2Y_{11}$ rb (n = 17 cells/3 humans), $Ca_V1.2$ (n = 19 cells/3 humans), AKAP5 (n

= 31 cells/3 humans), AC5 (n = 33 cells/3 humans), $PKA_{cat}$ (n = 21 cells/3 humans), $P2Y_{11}$ + AKAP5 (n = 25 cells/3 humans), $Ca_V1.2$ + AKAP5 (n = 24 cells/4 humans), AC5 + AKAP5 (n = 25 cells/3 humans), $P2Y_{11}$ + AC5 (n = 27 cells/3 humans), and $Ca_V1.2$ + $PKA_{cat}$ (n = 26 cells/3 humans). *$P$ < 0.05 with Kruskal-Wallis One-way ANOVA with specific Dunn's multiple comparisons as displayed. All significant $P$ values are < 0.0001. Data represent mean ± SEM. Source data are provided as Source Data file.

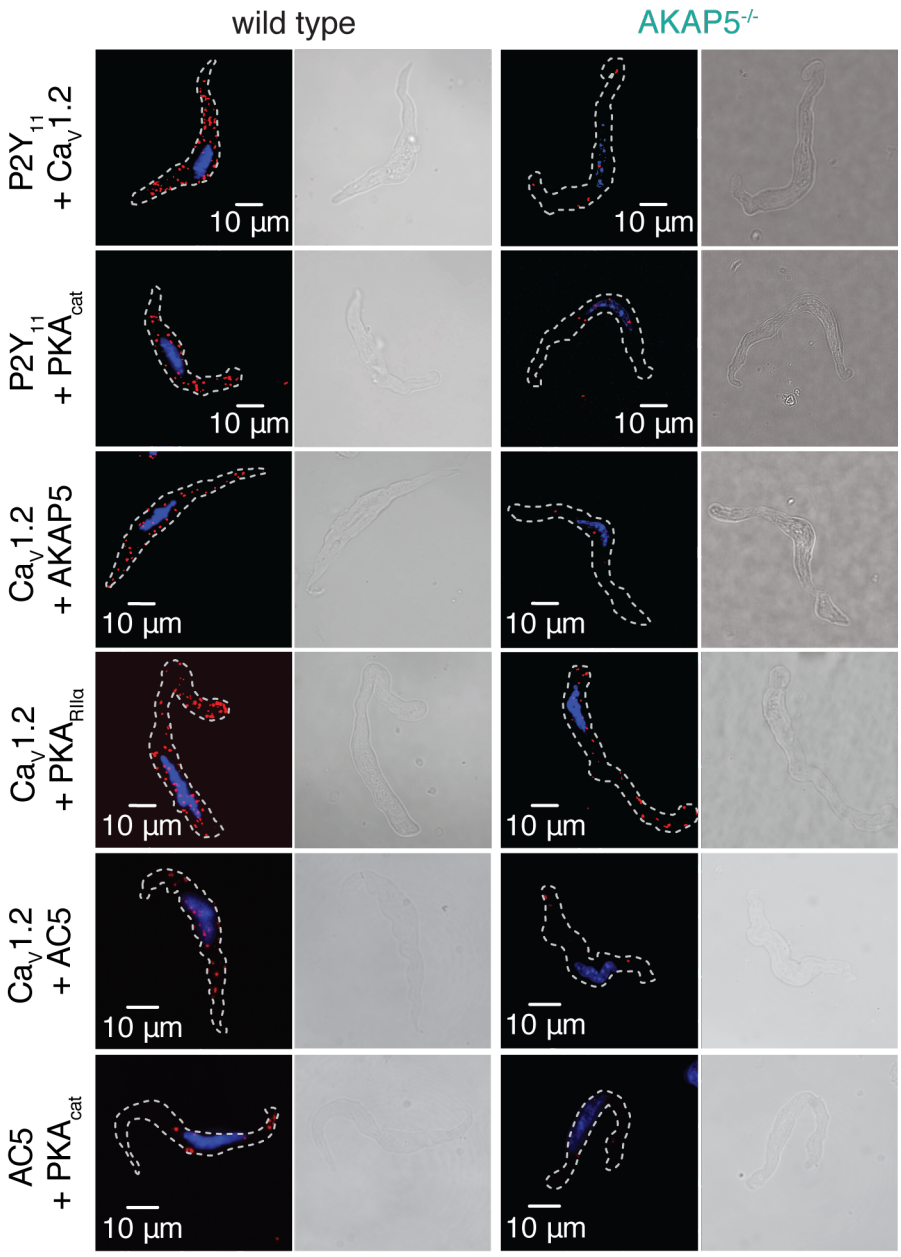


**Supplementary Figure 8. PLA images for WT and AKAP5$^{-/-}$ arterial myocytes.** Exemplary merged fluorescence proximity ligation assay (PLA; red)/nucleus (blue; left panels) and differential interference contrast (right panels) images of wild type (WT) and AKAP5$^{-/-}$ cerebral arterial myocytes co-labeled for $P2Y_{11}$ + $Ca_V1.2$, $P2Y_{11}$ + $PKA_{cat}$, $Ca_V1.2$ + AKAP5, $Ca_V1.2$ + $PKA_{RIIα}$, $Ca_V1.2$ + AC5 and AC5 + $PKA_{cat}$.

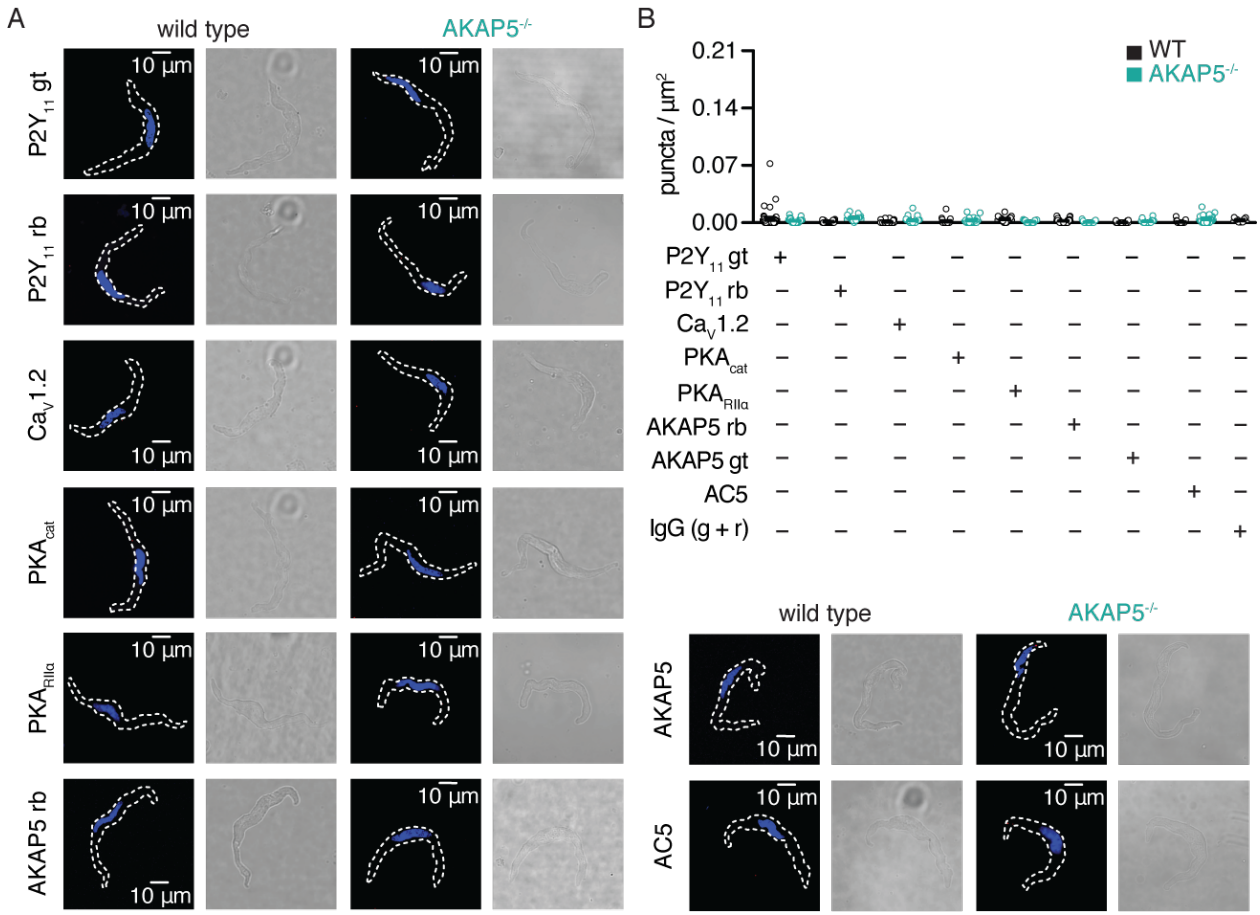


**Supplementary Figure 9. PLA images and quantification of negative control experiments for WT and AKAP5$^{-/-}$ arterial myocytes. A)** Representative merged fluorescence proximity ligation assay (PLA; red)/nucleus (blue; left panels) and differential interference contrast (right panels) images and **B)** quantification of PLA fluorescent puncta per cell area (puncta/µm$^2$) of wild type (WT) and AKAP5$^{-/-}$ arterial myocytes labeled with only one 1° antibody for $P2Y_{11}$ goat (gt; n = 43 cells/3 WT mice; n = 37 cells/3 AKAP5$^{-/-}$ mice), $P2Y_{11}$ rabbit (rb; n = 20 cells/3 WT mice; n = 17 cells/3 AKAP5$^{-/-}$ mice), $Ca_V1.2$ (n = 43 cells/3 WT mice; n = 34 cells/3 AKAP5$^{-/-}$ mice), $PKA_{cat}$ (n = 20 cells/3 WT mice; n = 18 cells/3 AKAP5$^{-/-}$ mice), $PKA_{RIIα}$ (n = 16 cells/3 WT mice; n = 15 cells/3 AKAP5$^{-/-}$ mice), AKAP5 rabbit (rb; n = 41 cells/3 WT mice; n = 15 cells/3 AKAP5$^{-/-}$ mice), AKAP5 goat (gt; n = 20 cells/3 WT mice; n = 18 cells/3 AKAP5$^{-/-}$ mice) and AC5 (n = 21 cells/3 WT mice; n = 26 cells/3 AKAP5$^{-/-}$ mice). For some experiments, WT arterial myocytes were labeled with primary goat and rabbit immunoglobulin G

(IgGs) followed by the PLUS and MINUS probes of the PLA assay (IgG (g + r) dataset; n = 9 cells/2 mice) as negative control experiments. Data represent mean ± SEM. Source data are provided as Source Data file.

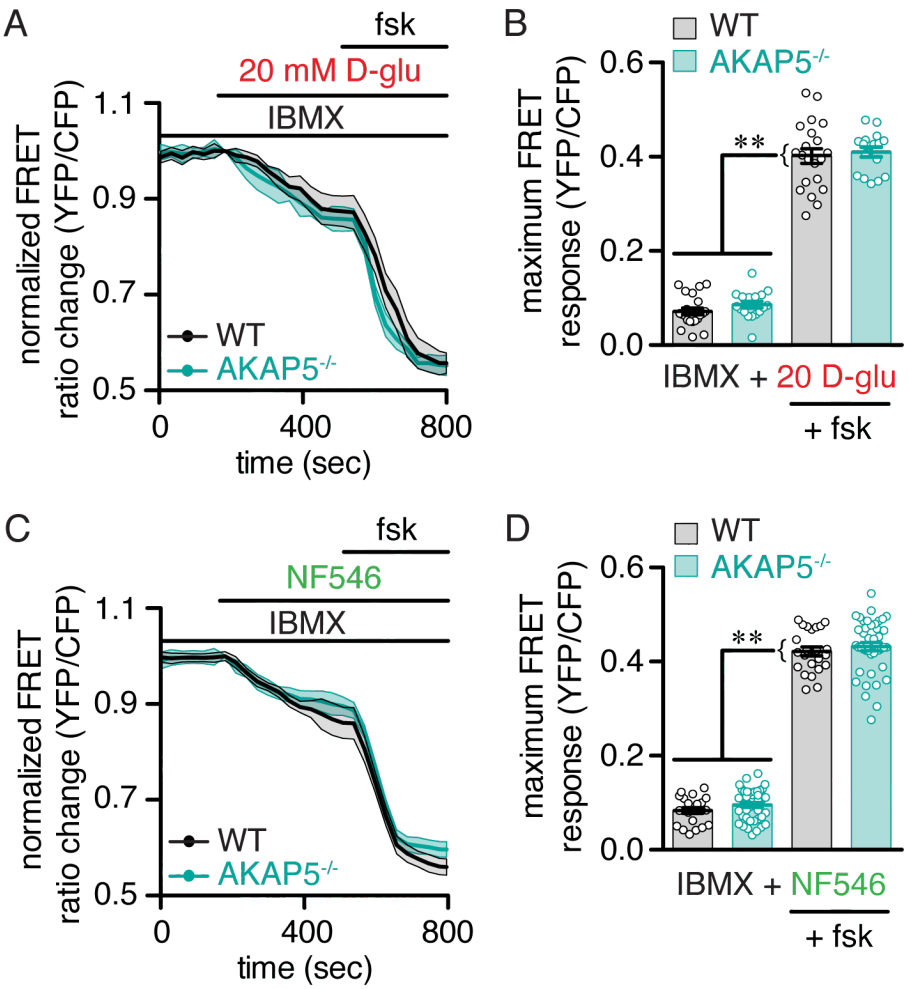


**Supplementary Figure 10. PDE inhibition rescues glucose/NF546-induced cAMP synthesis in arterial myocytes.** Time courses of the average ICUE3-PM traces (mean = solid line; SEM = shadow) and summary data of wild type (WT) and AKAP5$^{-/-}$ arterial myocytes pretreated with the broad phosphodiesterase (PDE) inhibitor 3-isobutyl-1-methylxanthine (IBMX) in response to **A, B)** 20 mM D-glucose (D-glu; n = 21 cells/3 WT mice and n = 17 arteries/3 AKAP5$^{-/-}$ mice) and **C, D)** NF546 (n = 23 cells/3 WT mice and n = 40 arteries/3 AKAP5$^{-/-}$ mice) and after application of forskolin. *$P$ < 0.05 with two-tailed Mann-Whitney test. The single asterisks highlight significant differences between datasets in the absence of forskolin. The double asterisks indicate a statistical difference within the same experimental group in the absence and presence forskolin. All significant $P$ values are < 0.0001. Data represent mean ± SEM. Source data are provided as Source Data file.

**Supplementary Table 1: Human nondiabetic patients undergoing surgical sleeve gastrectomy**

| age (years) | gender |
|---|---|
| 41.5 ± 5.0 | 5 F / 3 M |

Values are mean ± SEM. n = 8 samples obtained from 5 female and 3 male donors. Source data are provided as Source Data file.

**Supplementary Table 2: Percent treatment-induced changes in tone for experiments in Figure 3A and Figure 3D.**

| | WT (3A) | AKAP5$^{-/-}$ (3A) | WT (3D) | AKAP5$^{-/-}$ (3D) | AC5$^{-/-}$ (3D) |
|---|---|---|---|---|---|
| **peak 60 mM $K^+$ constriction (%)** | 67.4 ± 3.0 | 58.4 ± 8.0 | 62.2 ± 3.7 | 66.0 ± 2.9 | 69.9 ± 3.5 |
| **arterial tone (%) in 10 mM D-glu** | 16.1 ± 2.0 | 17.0 ± 1.7 | 14.6 ± 1.5 | 21.8 ± 3.4 | 15.9 ± 2.5 |
| **arterial tone (%) in 20 mM D-glu (3A) or NF546 (3D)** | 26.1 ± 2.7* | 19.5 ± 1.3 | 24.3 ± 3.1* | 21.7 ± 3.3 | 15.6 ± 2.6 |
| **Δ arterial tone (%)** | 10.0 ± 1.0* | 2.4 ± 1.1 | 9.8 ± 2.2* | -0.1 ± 0.5 | -0.2 ± 0.2 |

Values are mean ± SEM. For Figure 3A, n = 9 arteries from 5 WT mice and 7 arteries from 6 AKAP5$^{-/-}$ mice. For Figure 3D, n = 6 arteries from 4 WT mice, 8 arteries from 6 AKAP5$^{-/-}$ mice and 6 arteries from 4 AC5$^{-/-}$ mice. *$P$ < 0.05 with two-tailed Wilcoxon test for data associated with Figure 3A and Kruskal-Wallis One-way ANOVA with Dunn's multiple comparisons for data associated with Figure 3D. $P$ = 0.0039 for WT 10 mM D-glu-20 mM D-glu comparison in Figure 3Aii, $P$ = 0.0012 for WT-AKAP5$^{-/-}$ comparison in Figure 3Aiii, $P$ = 0.0313 for WT 10 mM D-glu-NF546 comparison in Figure 3Dii, and $P$ = 0.0036 for WT-AKAP5$^{-/-}$ and $P$ = 0.0040 for WT-AC5$^{-/-}$ for comparison in Figure 3Diii. Source data are provided as Source Data file.

**Supplementary Table 3: Percent treatment-induced changes in Figure 4.**

| **Percent treatment-induced changes in tone in Figure 4A and 4C** | | |
|---|---|---|
| | **WT** | **AKAP5$^{-/-}$** |
| **arterial tone (%) in 10 mM D-glu** | 24.5 ± 2.8 | 22.5 ± 2.7 |
| **arterial tone (%) in 10 mM D-glu + 10 mM mannitol** | 24.4 ± 3.1 | 23.5 ± 3.1 |
| **arterial tone (%) in 20 mM D-glu** | 45.1 ± 2.6* | 26.4 ± 2.8 |
| **arterial tone (%) in 20 mM D-glu + NF546** | 40.7 ± 1.8* | 22.9 ± 2.2 |
| **arterial tone (%) in 10 mM D-glu** | 23.1 ± 2.6 | - |
| **arterial tone (%) in NF340 + 10 mM D-glu + 10 mM mannitol** | 24.1 ± 3.0 | - |
| **arterial tone (%) in NF340 + 20 mM D-glu** | 21.8 ± 2.1 | - |
| **arterial tone (%) in NF340 + 20 mM D-glu + NF546** | 24.6 ± 2.3 | - |
| | | |
| **Percent treatment-induced changes in blood flow in Figure 4B** | | |
| **Δ blood flow in 10 mM D-glu + 10 mM mannitol** | 0.91 ± 0.01 | 1.01 ± 0.01 |
| **Δ in 20 mM D-glu** | 0.80 ± 0.02* | 0.97 ± 0.01 |
| **Δ in 20 mM D-glu + NF546** | 0.77 ± 0.03* | 1.00 ± 0.01 |

Values are mean ± SEM. For Figure 4A, n = 18 arteries from 3 WT mice and n = 21 arteries from 3 AKAP5$^{-/-}$ mice. For Figure 4B, n = 18 arteries from 5 WT mice and 12 arteries from 3 AKAP5$^{-/-}$ mice. For Figure 4C, n = 23 arteries from 3 WT mice. *$P$ < 0.05 with Friedman One-way ANOVA with Dunn's multiple comparisons. $P$ < 0.0001 for WT 10 mM D-glu-20 mM D-glu and $P$ = 0.0004 for WT 10 mM D-glu-20 mM D-glu + NF546 for comparisons in Figure 4A, and $P$ = 0.0007 for WT mannitol-20 mM D-glu and $P$ < 0.0001 for WT mannitol-20 mM D-glu + NF546 for comparisons in Figure 4B. Source data are provided as Source Data file.

**Supplementary Table 4: Percent treatment-induced changes in tone for experiments in Figure 7B.**

| | WT | AKAP5$^{-/-}$ |
|---|---|---|
| **peak 60 mM $K^+$ constriction (%)** | 66.7 ± 3.0 | 59.9 ± 3.7 |
| **arterial tone (%) in IBMX + 10 mM D-glu** | 15.7 ± 3.1 | 15.3 ± 2.1 |
| **arterial tone (%) in IBMX + 20 mM D-glu** | 26.5 ± 2.9* | 15.7 ± 2.3 |
| **arterial tone (%) in IBMX + 20 mM D-glu + NF546** | 26.5 ± 2.9* | 15.6 ± 2.4 |

Values are mean ± SEM. For Figure 7B, n = 6 arteries from 4 WT mice and 6 arteries from 3 AKAP5$^{-/-}$ mice. *$P$ < 0.05 with two-tailed Mann-Whitney test for 60 mM $K^+$ response and Friedman One-way ANOVA with Dunn's multiple comparisons for multiple comparisons. $P$ = 0.0281 for WT 10 mM D-glu + IBMX-20 mM D-glu + IBMX and $P$ = 0.0281 for WT 10 mM D-glu + IBMX-20 mM D-glu + NF546 + IBMX for comparisons in Figure 7B. Source data are provided as Source Data file.

**Supplementary Table 5: Key reagents/resources used in the study.**

| Reagent type (species) or resource | Designation | Source or reference | Identifiers | Additional Information |
|---|---|---|---|---|
| strain (*Mus musculus*), C57BL/6J | wild-type | Jackson Laboratories | stock # 000664 | |
| strain (*Mus musculus*) | AKAP5$^{-/-}$ | [1,2] | | Backcrossed for 10 generations into the C57BL/6J background |
| strain (*Mus musculus*) | AC5$^{-/-}$ | [3] | | Backcrossed for 10 generations into the C57BL/6J background |
| antibody | FP1 ($Ca_V1.2$; custom rabbit) | [4] | | 1:100 dilution. Used for mouse datasets. Validated in Davare et al, JBC doi: 10.1074/jbc.M005462200 and Buonarati et al F1000Res doi: 10.12688/f1000research.11808.2 |
| antibody | anti-$Ca_V1.2$ (mouse monoclonal) | Neuromab | clone N263/31 | 1:200 dilution. Used for human datasets. For validation see http://neuromab.ucdavis.edu/datasheet/N263_31.pdf |
| antibody | anti-AC5 (goat polyclonal) | Santa Cruz Biotechnology | sc74301 RRID: AB_2289217 | 1:50-1:1000 dilutions. Validated in Syed et al, JCI doi: 10.1172/JCI124705 |
| antibody | anti-$P2Y_{11}$ (rabbit polyclonal) | Abcam | ab180739 | 1:100-1:200 dilutions. Validated in Prada et al. eLife doi: 10.7554/eLife.42214 |
| antibody | anti-$P2Y_{11}$ (goat polyclonal) | Santa Cruz Biotechnology | sc-69588; clone C-18 | 1:100-1:200 dilutions. Prada et al. eLife doi: |

| | | | | |
|---|---|---|---|---|
| | | | RRID: AB_21559 | 10.7554/eLife.42214 |
| antibody | anti-AKAP79 (rabbit polyclonal) | Millipore | ABS102 | 1:200 dilution. For validation see https://www.emdmillipore.com/US/en/product/Anti-AKAP-79-Antibody,MM_NF-ABS102?ReferrerURL=https%3A%2F%2Fwww.google.com%2F |
| antibody | anti-AKAP150 (rabbit polyclonal) | Millipore | 07-210 | 1:200 dilution. Validated in Nystoriak et al, Science Signaling doi: 10.1126/scisignal.aaf9647 |
| antibody | anti-AKAP150 (goat polyclonal) | Santa Cruz Biotechnology | clone C-20 | 1:200 dilution. For validation see https://www.scbt.com/p/akap-150-antibody-c-20?productCanUrl=akap-150-antibody-c-20&_requestid=2603832,; additional information in https://datasheets.scbt.com/sc-377055.pdf |
| antibody | anti-$PKA_{RIIα}$ (mouse monoclonal) | BD Transduction Laboratories | 612242 | 1:50 dilution. Validated in Prada et al. eLife doi: 10.7554/eLife.42214 |
| antibody | anti-$PKA_{cat}$ α, β, γ (rabbit polyclonal) | Santa Cruz Biotechnology | sc-28892; clone H-95 | 1:200 dilution. For validation see http://datasheets.scbt.com/sc-28892.pdf |
| antibody | goat anti-rabbit IgG (H+L)- | Bio-Rad | 170-6515 RRID: AB_11125142 | 1:10000 dilution. For validation see https://www.bio- |

| | | | | |
|---|---|---|---|---|
| | horseradish peroxidase conjugate | | | rad.com/en-us/sku/1706515-goat-anti-rabbit-igg-h-l-hrp-conjugate?ID=1706515# |
| antibody | IRDye 800CW goat anti-mouse/rabbit | Abcam | ab216772/ ab216773 | 1:5000. For validation see https://www.abcam.com/goat-mouse-igg-hl-irdyereg-800cw-preadsorbed-ab216772.html and https://www.abcam.com/goat-rabbit-igg-hl-irdyereg-800cw-preadsorbed-ab216773.html |
| antibody | Alexa Fluor 430-conjugated goat anti-rabbit | Molecular Probes | A11064 RRID: AB_2534111 | 5 mg/mL dilution. For validation see https://www.thermofisher.com/antibody/product/Goat-anti-Rabbit-IgG-H-L-Cross-Adsorbed-Secondary-Antibody-Polyclonal/A-11064 |
| antibody | Alexa Fluor 568-conjugated donkey anti-mouse | Molecular Probes | A10037 RRID: AB_2534013 | 5 µg/mL dilution. For validation see Prada et al. eLife doi: 10.7554/eLife.42214; Nystoriak et al, Science Signaling doi: 10.1126/scisignal.aaf9647; Syed et al, JCI doi: 10.1172/JCI124705; https://www.thermofisher.com/antibody/product/Donkey-anti-Mouse-IgG-H-L-Highly- |

| | | | | |
|---|---|---|---|---|
| | | | | Cross-Adsorbed-Secondary-Antibody-Polyclonal/A10037 |
| antibody | Alexa Fluor 647-conjugated donkey anti-goat | Molecular Probes | A21447 RRID: 141844 | 5 µg/mL dilution. For validation see Prada et al. eLife doi: 10.7554/eLife.42214; Nystoriak et al, Science Signaling doi: 10.1126/scisignal.aaf9647; Syed et al, JCI doi: 10.1172/JCI124705; https://www.thermofisher.com/antibody/product/Donkey-anti-Goat-IgG-H-L-Cross-Adsorbed-Secondary-Antibody-Polyclonal/A-21447 |
| antibody | normal mouse IgG | Millipore | NI03 | 10 µg/mL dilution. For validation see https://www.emdmillipore.com/US/en/product/Normal-Mouse-IgG,EMD_BIO-NI03 |
| antibody | normal rabbit IgG | Cell Signaling | 2729S | 10 µg/mL dilution. For validation see https://www.cellsignal.com/products/primary-antibodies/normal-rabbit-igg/2729 |
| antibody | normal goat IgG | Millipore | NI02 | 10 µg/mL dilution. For validation see https://www.emdmillipore.com/US/en/product/Normal-Goat- |

| | | | | |
|---|---|---|---|---|
| | | | | IgG,EMD_BIO-NI02 |
| antibody | CD31 - biotin | BD Bioscience | 558737 RRID: AB_397096 | 5 mg/mL dilution. For validation see https://www.bdbiosciences.com/eu/applications/research/stem-cell-research/cancer-research/mouse/biotin-rat-anti-mouse-cd31-390/p/558737 |
| antibody | CD45 - biotin | BD Bioscience | 553077 RRID: AB_394607 | 2 µg/mL dilution. For validation see https://www.bdbiosciences.com/eu/applications/research/stem-cell-research/cancer-research/mouse/biotin-rat-anti-mouse-cd45-30-f11/p/553077 |
| antibody | lineage antibody cocktail | BD Bioscience | 559971 RRID: AB_10053179 | 2 µg/mL dilution. For validation see https://www.bdbiosciences.com/eu/applications/research/stem-cell-research/stem-cell-kits-and-cocktails/mouse/biotin-mouse-lineage-panel/p/559971 |
| FRET biosensor | ICUE3-PM/ ICUE3-NLS | [5,6] | | viruses/DNA constructs |
| chemical compound, drug | IBMX | Sigma | I5879 | |
| chemical compound, drug | mannitol | Fisher Scientific | BP686 | |
| chemical compound, drug | NF340 | Santa Cruz Biotechnology | sc-361274 | |
| chemical compound, drug | NF546 | Tocris | 3892 | |
| chemical compound, drug | nifedipine | Sigma-Aldrich | N7634 | |
| chemical compound, drug | forskolin | Sigma-Aldrich | F6886 | |

| | | | | |
|---|---|---|---|---|
| chemical compound, drug | amphotericin B | Sigma-Aldrich | A4888 | |
| chemical compound, drug | Duolink | Sigma | [7] | |
| software, algorithm | GraphPad Prism | | GraphPad Prism, RRID: SCR_002798 | v6 |
| software, algorithm | Origin | OriginLab | | v7.0 |
| software, algorithm | ImageJ | | Fiji, RRID: SCR_002285 | v1.51 |
| software, algorithm | pCLAMP10 | Molecular Devices | | v10.3; electrophysiology |
| software, algorithm | IonOptix | IonOptix | | v6.6; arterial diameter recordings |
| software, algorithm | Metaflor | Molecular Devices | | v7.7; FRET |
| software, algorithm | StCamSware | Sentech America Incorporated | | v3.10.0.3086 |
| hardware | Laser Speckle Contrast Imager | Moor Instruments | FLPI-2 | |
| software, algorithm | Moor FLPI Review | Moor Instruments | FLPI | v5.0 |
| software, algorithm | LASAF | Leica | | for GSD imaging |
| software, algorithm | Zen | Zeiss | | v2.3 SP1; for Airyscan imaging |
| software, algorithm | Fluoview | Olympus | | v1.4 |
| software, algorithm | CellQuest | BD Biosciences | | v5.2.1 |
| software, algorithm | FlowJo | Treestar Inc | | v9.9.6 |

**Supplementary References**


1. Navedo, M.F.*, et al.* AKAP150 is required for stuttering persistent Ca2+ sparklets and angiotensin II-induced hypertension. *Circ Res* **102**, e1-e11 (2008).
2. Nichols, C.B.*, et al.* Sympathetic stimulation of adult cardiomyocytes requires association of AKAP5 with a subpopulation of L-type calcium channels. *Circ Res* **107**, 747-756 (2010).
3. Timofeyev, V.*, et al.* Adenylyl cyclase subtype-specific compartmentalization: differential regulation of L-type Ca2+ current in ventricular myocytes. *Circ Res* **112**, 1567-1576 (2013).
4. Davare, M.A., Horne, M.C. & Hell, J.W. Protein phosphatase 2A is associated with class C L-type calcium channels (Cav1.2) and antagonizes channel phosphorylation by cAMP-dependent protein kinase. *J Biol Chem* **275**, 39710-39717 (2000).
5. Allen, M.D.*, et al.* Reading dynamic kinase activity in living cells for high-throughput screening. *ACS chemical biology* **1**, 371-376 (2006).
6. Liu, S., Zhang, J. & Xiang, Y.K. FRET-based direct detection of dynamic protein kinase A activity on the sarcoplasmic reticulum in cardiomyocytes. *Biochemical and biophysical research communications* **404**, 581-586 (2011).
7. Fredriksson, S.*, et al.* Protein detection using proximity-dependent DNA ligation assays. *Nature biotechnology* **20**, 473-477 (2002).